THE ASTROPHYSICAL JOURNAL, 314:397–403, 1987 March 1

WHERE MASSIVE STARS FORM: ASSOCIATED RADIO H II REGIONS AND CO CLOUDS IN THE NORTHERN MILKY WAY[1]

W. H. WALLER
University of Massachusetts, Amherst
D. P. CLEMENS
University of Arizona, Tucson
AND
D. B. SANDERS AND N. Z. SCOVILLE
California Institute of Technology
Received 1985 December 2; accepted 1986 August 25

ABSTRACT

The sites of massive star formation in molecular clouds are investigated by comparing high-resolution radio surveys of molecular and ionized gas emission in the Milky Way. CO emission maps from the Massachusetts–Stony Brook survey of the first Galactic quadrant are used to locate, in l, b, and v, the molecular clouds associated with radio recombination-line H II regions. We find that the radio H II regions are typically associated with giant molecular clouds (GMCs) with diameters of 20–60 pc and virial masses of 10^5–10^6 $M_\odot$. The radio H II regions appear preferentially concentrated toward the centers of the GMCs, contrary to the "blister" picture of massive star formation on cloud surfaces.

Subject headings: interstellar: molecules — nebulae: H II regions — stars: formation

I. INTRODUCTION

Surveys of OB associations, H II regions, and molecular clouds in the Galaxy have revealed a strong link between molecular clouds and massive star formation (Scoville and Solomon 1973; Fich, Treffers, and Blitz 1982; Sanders, Scoville, and Solomon 1985). One frequently cited prescription for this link is the "blister" model of massive star formation, in which massive stars form on the surfaces of molecular clouds as a result of external perturbations (e.g., Israel 1978; Herbst and Assousa 1977). Evidence in favor of this model, however, has come primarily from optical surveys of H II regions which were subject to the obscuring effects of dust and hence were biased toward those nearby H II regions that are located on the near surfaces of clouds.

To determine the spatial and kinematic relationship between molecular clouds and massive stars, we compare well-sampled emission surveys of CO and radio H II regions in the Milky Way. The molecular clouds are most effectively mapped via the 2.6 mm spectral-line emission of CO, which has proven an excellent tracer of H_2 throughout the Galaxy (Scoville and Solomon 1975). The ionized sites of massive star formation are best located at radio wavelengths, where continuum and recombination-line surveys are capable of detecting the H II regions associated with OB star formation—whether the H II regions lie outside or inside dusty clouds.

In this paper, spatial and kinematic measurements of 54 radio H II regions and their associated molecular clouds are presented. The resulting distributions of relative position and velocity favor a picture of "embedded" H II regions which have not drifted significantly from their original birth sites.

II. SURVEY DATA

The molecular cloud data were taken from the Massachusetts–Stony Brook survey of CO emission in the first Galactic quadrant (Sanders *et al.* 1986). The CO survey includes 40,551 spectra obtained on a 3′ × 3′ grid in l and b for the longitudes 18°–55°, where the extent in latitude was −1°.05 to +1°.00, and on a 6′ × 6′ grid for the longitudes 8°–18° and 55°–90°, where the latitude extent was −1°.00 to +1°.00. For the present study, molecular clouds were identified from the survey as having CO antenna temperatures T_R^* higher than 2 K (~5 σ). This cutoff in antenna temperature roughly corresponds to a 10 K km s^{-1} cutoff in integrated CO intensity or a 4 mag lower limit in visual extinction, assuming a CO to H_2 conversion factor of 4×10^{20} cm^{-2} (K km s^{-1})$^{-1}$ (Sanders, Scoville, and Solomon 1985).

The H II region data were based on the Bonn survey of 6 cm radio continuum emission in the first Galactic quadrant (Altenhoff *et al.* 1978). Kinematic data for the selected sources were obtained from hydrogen recombination-line observations of the strong continuum peaks found by the Bonn survey. Most of the data (84%) were obtained from the H110α survey of Downes *et al.* (1980), where kinematic distance ambiguities had been removed by comparing the H110α emission-line velocities with H_2CO and H I absorption-line velocities observed along the same line of sight. Additional recombination-line data were taken from a similar compilation of H109α sources by Lockman (1979) and from an ongoing survey of H85α sources (F. J. Lockman, private communication) whose distance ambiguities remain unsolved. The final selection of 56 recombination-line sources was based solely on the availability of corresponding CO maps at the time of this investigation (before completion of the CO survey). An automated study involving a much larger sample of CO clouds—with and without H II regions—is in preparation (Scoville *et al.* 1987). The unique features of the present study include the use of (b, v)-diagrams to measure cloud sizes down to a constant 2 K threshold of antenna temperature (the automated study can only measure down to the 4 K level before cloud blending begins to subvert the algorithm) and the development of theo-

[1] *Contributions of the Five College Astronomy Department*, No. 618.

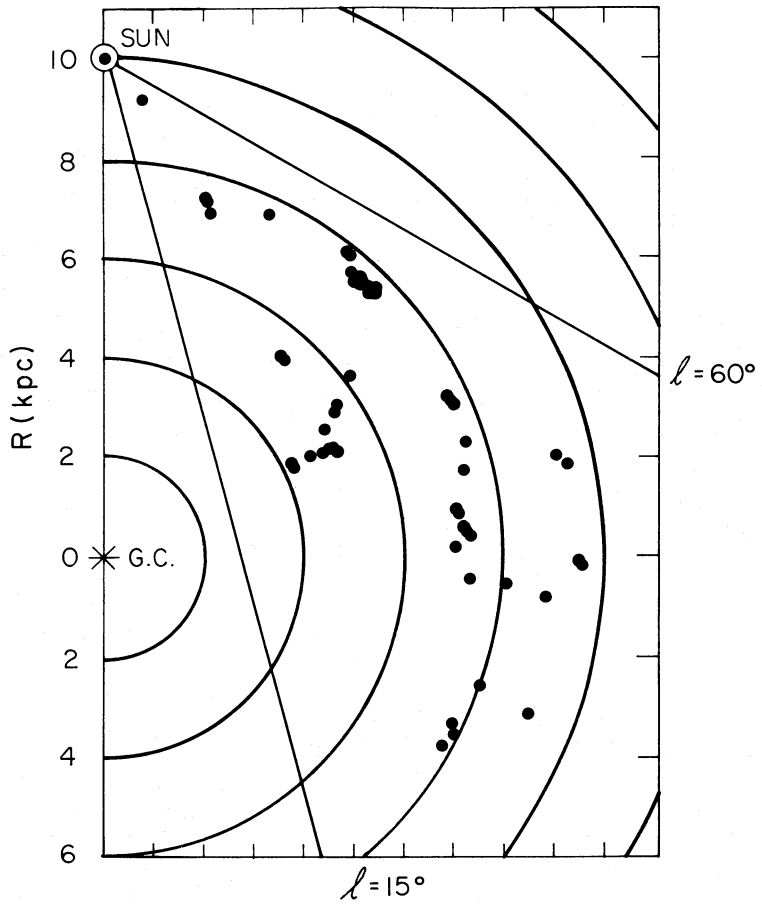

FIG. 1.—Projected face-on distribution of sample radio H II regions in the first Galactic quadrant

retical models against which the observed distribution of H II region locations can be compared.

Figure 1 shows the distribution in the Galactic disk of the 51 H II regions having resolved distances. The majority of these H II regions are located in the molecular cloud ring between $R = 5$ and 8 kpc (assuming a radius of 10 kpc for the solar circle). About one-third of the Downes sources qualify as giant H II regions, i.e., having luminosities at 5 GHz greater than 400 Jy kpc^2, and thus would be detectable out to distances of 20 kpc—the far edge of the inner Galaxy. Of the remainder, only six sources are less luminous at 5 GHz than the Orion nebula [L(Orion) $\approx$ 110 Jy kpc^2]. The "typical" H II region in the sample has a diameter of $\sim$10 pc, a number density of $\sim$100 H$^+$ cm^{-3}, and an age of $\sim 10^5$ yr. Israel classifies such objects as "classical" or class IV H II regions (Habing and Israel 1979). The young ages, in particular, enable the radio H II regions in the present sample to be used as accurate tracers of recent massive star formation.

III. H II–CO ASSOCIATIONS

To analyze the spatial and kinematic relationships between H II regions and CO clouds, the peak positions of the radio recombination-line emission peaks were plotted onto spatial-velocity (b, v)-maps of CO emission generated from the Massachusetts–Stony Brook survey. Unlike (l, b)-maps of integrated intensity that have been used in previous H II–CO studies (cf. Myers *et al.* 1986), the (b, v)-diagrams used here are not binned over some finite velocity interval. Therefore, they can be used to probe CO structures down to the 3′ × 3′ × 1 km s^{-1} resolution limit of the Massachusetts–Stony Brook survey. The chances of mistaking two separate clouds as one composite feature are thus minimized.

The criteria used to associate a radio H II region with a particular CO cloud were:

1. The (l, b, v)-position of the H II region had to lie within the 2 K contour of the CO cloud. If this first condition was not met, then we required that:
2. The difference in radial velocity between the H II region and the nearest 2 K contour of the CO cloud (as measured along the line of sight of the H II region) had to be less than 3 km s^{-1}; and
3. the difference in longitude and latitude between the H II region and the nearest 2 K contour of the CO cloud had to be less than 0°.2, as measured at the radial velocity of the H II region.

The last two criteria were chosen to overcome the degree of cloud crowding apparent in the (b, v)-maps (see Fig. 2). Referring the H II regions to the 2 K boundaries rather than to the centroids of the clouds enabled H II–CO associations to be identified without prior knowledge of each cloud's size and shape. A total of 54 H II region–CO cloud associations (all but two of the plotted sample) were found to meet the above criteria.

IV. PROPERTIES OF MOLECULAR CLOUDS WITH H II REGIONS

Once an associated cloud was identified, its physical properties were measured from the maps. Angular extents in longitude and latitude were based on the 2 K temperature contours

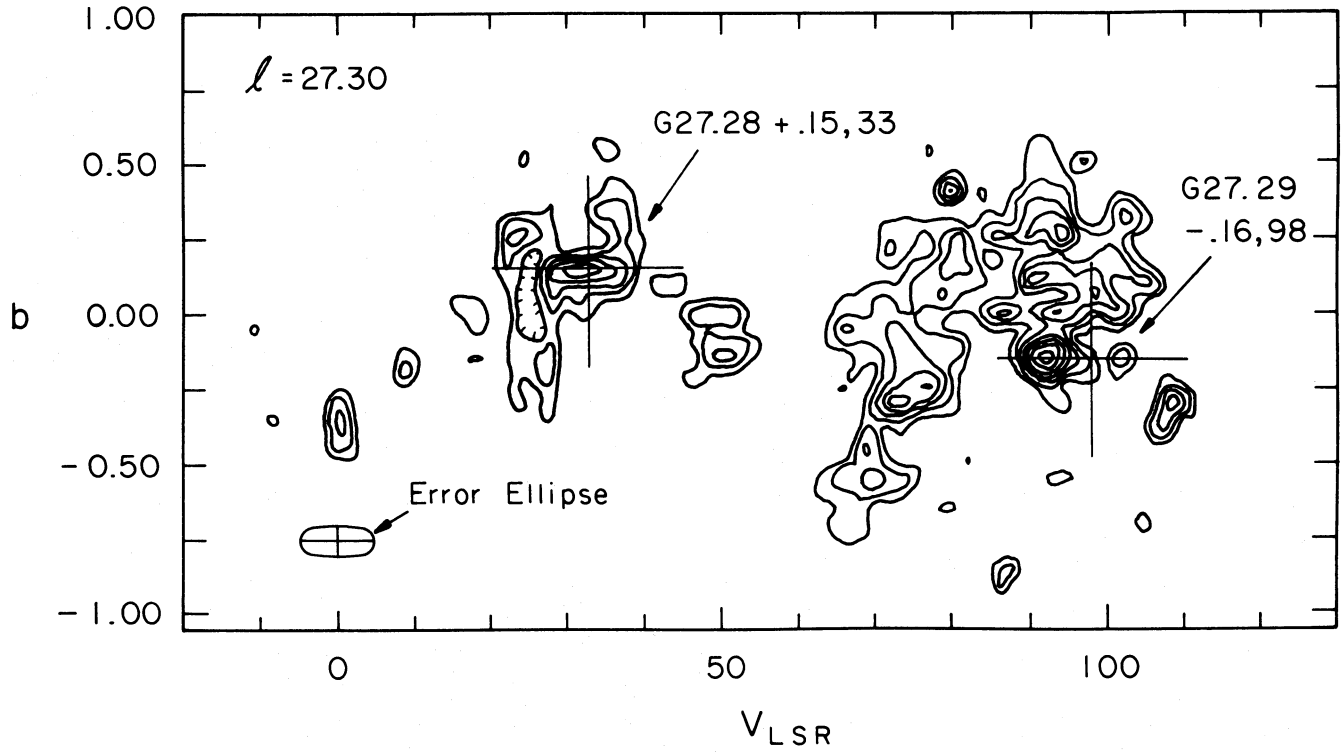

FIG. 2.—A representative latitude-velocity (b, v)-map of CO radiation temperature taken from the Massachusetts–Stony Brook Galactic plane survey. The lowest contour of emission is at $T_R^* = 1.25$ K with the higher contours at $T_R^* = 2, 3, 4, 5, \ldots$ K. The positions of two radio H II regions are plotted on the (b, v)-map along with the estimated positional error ellipse. The H II region at lowest velocity (G27.28+0.15, 33 km s^{-1}) is located at the emission peak of its associated CO cloud, whereas the H II region at higher velocity (G27.29−0.16, 98 km s^{-1}) is significantly redshifted from the emission peak of the nearest CO cloud. Since the latter H II region is located within 3 km s^{-1} of the cloud's 2 K contour, the H II–CO association was considered valid.

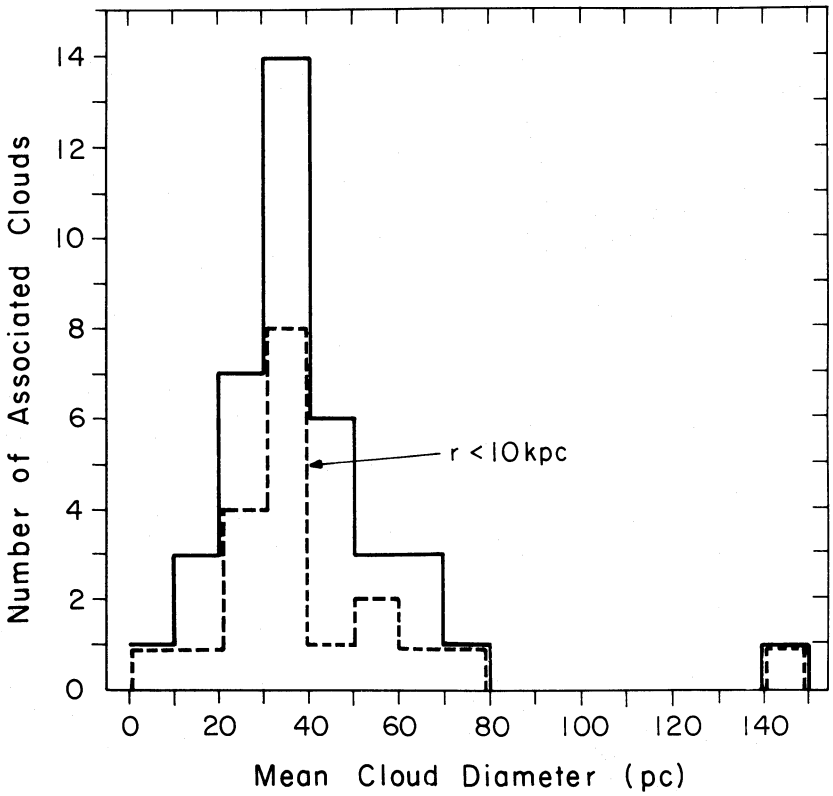

FIG. 3.—Distribution of mean diameters for the associated CO clouds, where the mean diameter is an average of the extents in longitude and latitude. Dashed histogram includes only clouds closer than 10 kpc which are resolved down to ~18 pc. Solid histogram includes all the associated clouds.

in the (b, v)-maps (rather than the FWHP extents, which are sensitive to local heating effects), and the centroid position and mean diameter of the cloud were derived from the angular extents. The 2 K boundaries were also used by Sanders, Scoville, and Solomon (1985) in their study of CO cloud properties; thus the present study can be directly compared with their results. The centroid velocity and mean velocity width (at both the 2 K and FWHP levels) were obtained from the (b, v)-maps by averaging several measurements taken near the (l, b)-centroid of the cloud. The (b, v)-diagrams were also used to obtain the position and antenna temperature (T_p) of the peak CO emission associated with each H II region in the cloud. Of the 54 H II–CO associations, 51 involved H II regions whose near/far distance ambiguities could be resolved—either via absorption line observations (Downes *et al.* 1980; Lockman 1979) or by association with a cloud which contained another H II region whose distance ambiguity was resolved via the absorption line measurements. The distances obtained to these H II regions were used to transform the angular measurements of each associated cloud into absolute displacements and sizes. The measured and derived properties for each of the H II–CO associations are listed in Table 1.

Figure 3 shows the distribution of mean diameters for the associated clouds. The dashed-line histogram indicates the size distribution for clouds which are closer than 10 kpc and hence are resolved down to 18 pc sizes. Size uncertainties, due to uncertain kinematic distances (typically 1 kpc) and uncertain angular extents (0°.07) are estimated at 10 pc.

The peak and median of the distribution of cloud sizes both occur at $\sim$35 pc. By comparison, the overall cloud-size distribution for the inner Galaxy is characterized by a single power law with a median value of 25 pc and no turnover apparent at the 18 pc resolution limit (Sanders, Scoville, and Solomon 1985). Comparison of these findings suggests that radio H II regions occur preferentially in the largest clouds, a finding also noted by Myers *et al.* (1986).

An important constraint on the mass density of the clouds is provided by the empirical correlation of the measured sizes and velocity widths. If the clouds are relaxed and there is a balance between the gravitational and kinetic energies, then the virial theorem can be used to estimate the typical mass densities for the GMCs. The empirical size–line width relationship for the clouds associated with the radio H II regions can be adequately represented by the following power law:

$$\Delta v(\mathrm{FWHM}) = (0.77 \pm 0.24)(D/\mathrm{pc})^{(0.62\pm0.15)}\ \mathrm{km\ s^{-1}}\ , \quad (1)$$

a relation which is very close to that found by Sanders, Scoville, and Solomon (1985) ($\Delta v = 0.88 D^{0.62}$ km s^{-1}), using latitude chords through 80 clouds. The present sample has the virtue that all the clouds have well-determined distances. Substituting the power-law representation into the virial relationship for a spherical cloud of uniform density gives $M \approx 3.2 \times 10^5 (D/35\ \mathrm{pc})^{2.24}\ M_\odot$. A 20 pc cloud would have a mass of $9 \times 10^4\ M_\odot$ and a mean number density of 330 H_2 cm^{-3}, assuming a helium abundance of 0.26. The very large GMCs of diameter 80 pc would have virial masses of $2.1 \times 10^6\ M_\odot$ and mean number densities of 115 H_2 cm^{-3}.

V. H II REGION LOCATIONS

a) Projected Positions

To determine the location of H II regions with respect to their parent clouds, each cloud was modeled as an ellipse having a semimajor axis of $\Delta l/2$ and a semiminor axis of $\Delta b/2$. The offset $a_{\mathrm{H\,II–CO}}$ of the H II region with respect to the centroid of its associated cloud was normalized to the size of the cloud and is given by

$$a_{\mathrm{H\,II–CO}} = \left[\frac{(l_{\mathrm{H\,II}} - l_{\mathrm{CO}})^2}{(\Delta l_{\mathrm{CO}}/2)^2} + \frac{(b_{\mathrm{H\,II}} - b_{\mathrm{CO}})^2}{(\Delta b_{\mathrm{CO}}/2)^2}\right]^{1/2} . \quad (2)$$

Since the analysis of relative position does not require knowledge of distances, all 54 H II–CO associations could be considered. However, eight of the associations involved poorly resolved clouds and hence were dropped from the analyzed sample. The resulting distribution of offsets is shown as the shaded histogram in Figure 4. The average uncertainty of the binned offsets is $\sim \pm 0.2$, which corresponds to the bin width in the histogram. The median and peak of the distributions both occur at $a_{\mathrm{H\,II–CO}} = 0.5 \pm 0.1$, a result which immediately differs with the "limb-brightened" profiles anticipated by the blister picture (cf. Israel 1978).

To estimate the corresponding three-dimensional distribution, the observed distribution was compared with those obtained from a spherical cloud model which contains a spherically symmetric distribution of H II regions. The crucial parameter in the model is the probability density $\rho(r)$ for an H II region to exist at radius r. For example, if there is an equal probability for an H II region to exist anywhere inside a GMC, then $\rho(r)$ = constant. The resulting distribution of projected positions for this case shows a peak at offset $a_{\mathrm{H\,II–CO}} \approx 0.7$, which is more skewed toward the projected edge of the cloud than the observed distribution. A probability density that favors the surface layers of the cloud would further skew the projected distribution toward larger offsets. The spherical models that best match the observed distribution within $a_{\mathrm{H\,II–CO}} = 1.0$ have $\rho(r) \propto r^{-1}$ to r^{-2}, i.e., centrally concentrated distributions, with the $1/r$ density law yielding the minimum χ^2 deviation at the 99% confidence level (assuming Poisson noise statistics).

Proper treatment of those H II regions situated *beyond* the 2 K boundaries of their associated molecular clouds is difficult. Since the radio H II regions are young [τ(H II) $\approx 5 \times 10^5$ yr], their exciting stars cannot have drifted much more than 5 pc from their birth sites (assuming a stellar velocity dispersion of 10 km s^{-1}, equivalent to the typical velocity width of the clouds in the present sample; cf. Jones and Herbig 1979; Fich, Treffers, and Blitz 1982). Therefore, an outlying H II region probably does not represent an itinerant OB association but rather a parcel of ionized gas that was once in molecular form near the surface of its host cloud. If the H II region is included as part of its associated cloud, its position can then be modeled along with the other H II regions. One approach, yielding the most favorable assessment of the peripheral H II region hypothesis, is to assign all nine of the outlying H II regions to the surfaces of their corresponding clouds (i.e., to the $a_{\mathrm{H\,II–CO}} =$ 0.8–1.0 bin). The corresponding three-dimensional distribution is then best modeled by superposing two sets of probability density laws—a radially decreasing density law, which accounts for $\sim$70% of the H II–CO associations, plus a density law favoring the cloud peripheries, which accounts for the remaining 30%. The dominance of the radially decreasing mode is supported by a χ^2 test of the spherical power-law models which once again yields minimum deviation at the 99% confidence level with the $1/r$ density law. If the outlying H II regions were once inside their clouds and have since dis-

TABLE 1

H II–CO Associations

l(H II)[a] (1)	b(H II)[a] (2)	v(H II)[b] (km s^{-1}) (3)	l(CO)[c] (4)	b(CO)[c] (5)	v(CO)[c] (km s^{-1}) (6)	d(H II)[d] (kpc) (7)	L(H II)[e] (Jy kpc^2) (8)	T_p(CO)[f] (K) (9)	Δl(CO)[c] (10)	Δb(CO)[c] (11)	D(CO)[c] (pc) (12)	Δv(CO)[c] (km s^{-1}) (13)	R[g] (kpc) (14)	Notes (15)
24°.80	+0°.10	107	24°.77	+0°.05	107	9	575	9	0°.25	0°.26	40	10	4.3	
24.81	+0.10	114 ± 2	24.80	+0.10	115	9	932	10	0.10	0.09	15	8	4.3	1
26.10	−0.07	33	26.20	+0.00	30	15	1220	3	0.10	0.12	29	3	7.7	
26.98	−0.07	79	26.72	−0.07	81	...	...	6	0.45	0.20	...	8	5.6	
27.28	+0.15	33	27.20	+0.13	33	15	280	7	0.30	0.15	60	12	7.8	
27.29	−0.16	98 ± 4	27.32	−0.14	92	9	610	8	0.25	0.17	33	9	4.8	
27.49	+0.19	35	27.52	+0.19	37	15	675	8	0.15	0.10	33	11	7.7	
28.80	+0.17	108	28.80	+0.17	108	9	150	7	0.10	0.18	22	9	4.8	2
28.82	−0.23	90 ± 1	28.82	−0.26	87	...	...	11	0.15	0.19	...	8	5.1	2
29.94	−0.04	98	29.90	−0.08	98	9	1340	12	0.50	0.51	80	20	5.1	
30.23	−0.14	99	30.65	−0.10	100	9	210	10	0.90	1.00	143	21	5.1	2, 3
30.39	−0.24	103 ± 1	30.65	−0.10	102	9	373	10	0.90	1.00	143	23	5.1	2, 3
30.69	−0.26	98	30.65	−0.10	93	9	240	9	0.90	1.00	143	30	5.2	2, 3
30.78	−0.03	90 ± 2	30.65	−0.10	97	7	3050	14	0.90	1.00	143	35	5.5	2, 3
30.85	+0.13	98 ± 2	30.65	−0.10	98	7	...	14	0.90	1.00	143	35	5.5	2, 3
30.85	+0.13	36 ± 4	30.90	+0.15	39	15	...	6	0.20	0.30	64	15	7.8	4
32.80	+0.19	17	32.77	+0.19	17	16	900	3	0.15	0.05	27	8	9.0	1
33.12	−0.08	97 ± 3	33.03	−0.05	100	8	529	5	0.45	0.30	55	13	5.5	2
33.91	+0.11	98	33.95	+0.03	100	8	76	4	0.20	0.15	25	8	5.6	2
34.25	+0.14	53	34.20	+0.15	59	4	183	7	0.50	0.58	35	13	7.2	2, 5
35.04	−0.50	52	35.07	−0.48	50	13	274	7	0.15	0.25	44	9	7.5	2
35.59	−0.49	59 ± 4	35.60	−0.54	56	12	...	4	0.10	0.07	18	4	6.9	2, 6
35.60	−0.03	50	35.55	−0.03	50	3	39	7	0.50	0.55	32	17	7.4	2, 5
35.66	−0.03	53	35.55	−0.03	50	3	77	7	0.50	0.55	32	17	7.3	2, 5
37.36	−0.23	39	37.27	−0.23	37	13	192	5	0.15	0.17	37	8	8.0	1
37.37	−0.07	57	37.42	−0.04	57	12	523	5	0.15	0.07	23	6	7.2	1
37.44	−0.04	61	37.42	−0.04	57	12	609	5	0.15	0.07	23	6	7.2	1
37.54	−0.11	55	37.55	−0.09	53	12	302	8	0.10	0.09	20	8	7.3	1
37.67	+0.13	86	37.55	+0.13	85	8	180	5	0.50	0.40	63	12	6.1	2
37.76	−0.22	61	37.77	−0.19	60	11	516	7	0.15	0.15	30	8	7.1	1
37.87	−0.40	60	37.85	−0.40	62	11	727	5	0.30	0.20	50	10	7.1	
39.25	−0.06	23	39.25	−0.09	22	14	444	8	0.15	0.13	34	11	8.5	6
41.10	−0.21	58	41.20	−0.26	60	11	523	8	0.40	0.30	67	10	7.4	2, 6
41.52	+0.03	15	41.77	+0.05	15	1	2	5	0.40	0.25	6	6	9.2	
43.17	+0.00	10 ± 2	43.20	−0.04	10	14	10105	5	0.20	0.16	44	17	9.5	7
43.18	−0.52	56	43.07	−0.52	58	10	99	6	0.35	0.17	48	8	7.5	6
43.23	−0.05	9	43.20	+0.00	10	14	406	5	0.20	0.16	44	17	9.5	7
45.12	+0.14	57	45.17	+0.10	58	10	630	7	0.25	0.13	32	10	7.6	
45.45	+0.06	54	45.47	+0.03	58	10	800	9	0.25	0.35	51	14	7.7	
45.47	+0.13	54	45.47	+0.03	58	10	226	9	0.25	0.35	51	14	7.7	
46.49	−0.25	57	46.30	−0.20	53	4	91	5	0.60	0.30	35	7	7.6	
48.60	+0.04	17	48.62	+0.05	19	12	1138	10	0.15	0.20	37	13	9.2	2
48.64	+0.23	13	48.67	+0.20	12	12	408	6	0.25	0.14	42	8	9.4	2, 6
48.93	−0.29	66	48.95	−0.30	68	7	553	11	0.30	0.10	23	10	7.5	2, 8
49.06	−0.26	60	48.95	−0.30	68	7	157	9	0.30	0.10	23	10	7.6	2, 8
49.08	−0.38	68	48.95	−0.30	68	7	205	9	0.30	0.10	23	12	7.6	2, 8
49.20	−0.35	67	49.35	−0.35	67	7	900	8	0.40	0.20	34	13	7.6	2, 8
49.38	−0.30	52	49.50	−0.32	53	7	1810	10	0.40	0.30	43	12	7.9	2, 8
49.41	−0.19	46	49.30	−0.12	46	7	597	8	0.20	0.25	27	10	8.1	2, 8
49.44	−0.46	59	49.45	−0.32	58	7	274	15	0.30	0.30	37	12	7.7	2, 8
49.49	−0.38	57 ± 2	49.45	−0.32	58	7	6390	17	0.30	0.30	37	16	7.7	2, 8
51.06	+0.16	42 ± 4	50.82	+0.19	44	...	...	4	0.35	0.18	...	6	8.3	
51.20	+0.07	55	51.37	+0.00	55	6	1468	3	0.45	0.25	38	10	7.8	
51.36	+0.00	59	51.37	+0.00	55	6	133	7	0.45	0.25	38	9	7.9	

[a] Tolerance ±0°.05.
[b] Tolerance ±5 km s^{-1} except where noted.
[c] For cloud centroid or (Δ values) extent of cloud, as defined by the $T_R^* = 2$ K contour; tolerances: (l, b) ±0°.07, (v) ±1.4 km s^{-1}, (D) ±10 pc.
[d] Distance of region and its associated cloud (±1 kpc).
[e] Tolerance ±100 Jy kpc^2.
[f] Tolerance ±1 K.
[g] Galactocentric radius of H II region and its associated CO cloud (±1 kpc).

Notes.—(1) Marginally resolved cloud. (2) Possible blending difficulties. (3) W43 cloud complex. Diameter is based on $d = 8.60$ kpc. (4) Cloud in a larger cluster ($D \approx 197$ pc) which, in turn, may be part of a kpc-long far-side chain. (5) Part of the W44 cloud cluster. Cluster centroid is at (G35.22−0.03, 50 km s^{-1}). Longitudinal extent is 2°.5. (6) Distance ambiguity due to lack of H_2CO absorption at higher velocities. Near/far decision is based on the presence/absence of CO emission at higher velocities and on the angular extent of the associated cloud. (7) The W49A associations. The CO velocity width and centroid refer to the entire complex, not to the individual cloud components. (8) The W51 associations.

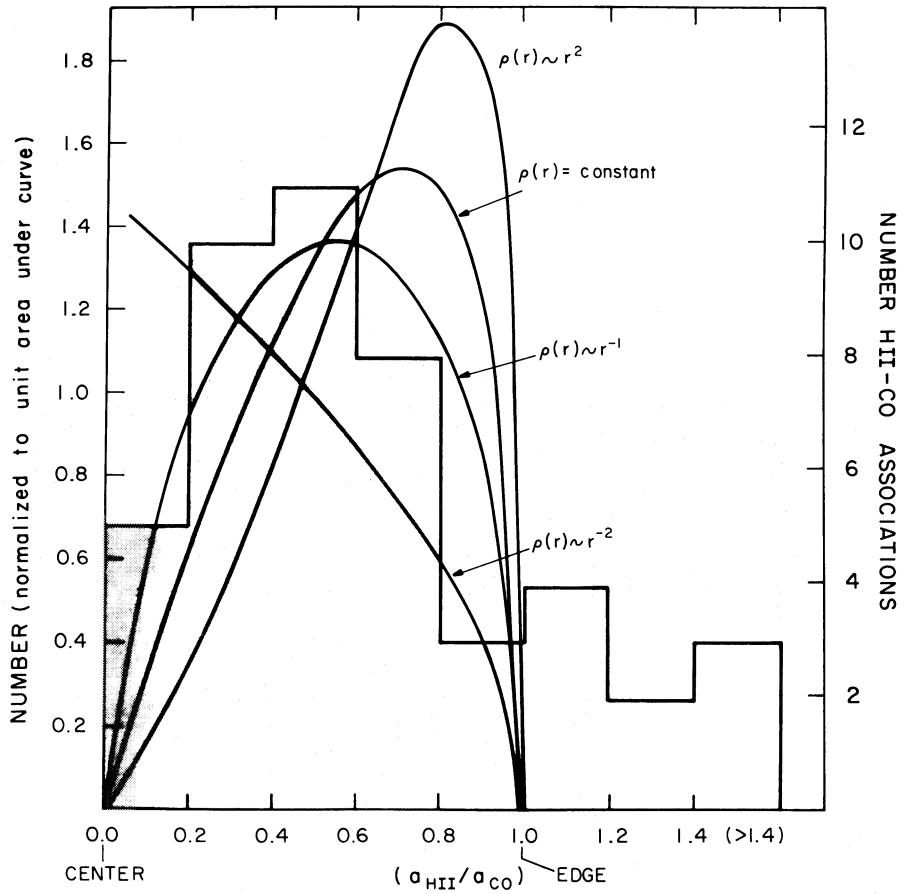

FIG. 4.—Distribution of projected angular offsets $a_{\text{H II–CO}}$ of the H II regions from the cloud centroids. For each cloud, the offset is normalized by the cloud size. An offset of zero corresponds to the H II region residing at the projected centroid of its cloud; a ratio of unity places the H II region at the cloud edge. Curves based on spherically symmetric models of clouds containing H II regions are also displayed. Each curve is normalized via the total area beneath it.

rupted the clouds to a large extent, then they would be binned into a larger range of $a_{\text{H II–CO}}$ than the above 0.8–1.0 range. The percentage of peripheral H II regions would then be reduced from the 30% value.

b) Kinematic Relations

Radial velocity differences between radio H II regions and their associated CO clouds provide a measure of how rapidly the H II gas is flowing away from the molecular gas. Figure 5 shows the distribution of velocity differences between the H II regions and their host clouds. The distribution is centrally peaked, having a mean velocity difference of -0.1 ± 0.4 km s^{-1}, similar to that found by Myers *et al.* (1986). This result indicates that the H II gas has random trajectories with respect to the molecular gas, unlike the situation with optically selected H II regions, where preferentially blue-shifted H II flows are observed, presumably due to ionized gas on the near surfaces of the molecular clouds (Fich, Treffers, and Blitz 1982; Israel 1978).

The rms dispersion of the velocity difference is 2.8 km s^{-1}, or roughly 3 times smaller than the cutoff imposed by the second association criterion discussed in § III (assuming a mean 2 K velocity width of 10 km^{-1}). Therefore, the kinematic restriction on association has not significantly biased the kinematic results. The dispersion, however, could be entirely due to the 2–5 km s^{-1} uncertainty in the hydrogen recombination-line measurements. Nevertheless, it provides an upper limit on the rms flow velocity of the ionized gas with respect to the molecular gas. Multiplying the dispersion by $3^{1/2}$ yields a three-dimensional rms flow velocity of 5.0 km s^{-1}. At this velocity, the centroid of the ionized gas will flow only 2.6 pc from its molecular antecedent during a typical 5×10^5 yr H II region lifetime. It should be noted that the motion of the exciting stars relative to the molecular gas contributes nothing to the velocity difference between the ionized gas and molecular gas. Since the velocity differences between the ionized and molecular gas *and* between the stars and molecular gas (Jones and Herbig 1979; Fich, Treffers, and Blitz 1982) are both low, the observed positions of the H II regions satisfactorily represent—to within the resolutions of the CO and radio continuum surveys—the original birth sites of the massive stars.

VI. SUMMARY

This study of associations between radio H II regions and CO clouds has shown that the formation of massive stars occurs predominantly in the interiors of the larger, GMCs. The resulting "embedded" picture of massive star formation conflicts with the "blister" picture exemplified by the Orion H II–CO association. The embedded geometry further suggests that external triggering from spiral density-wave shocks and supernova blast waves may not be essential to creating massive

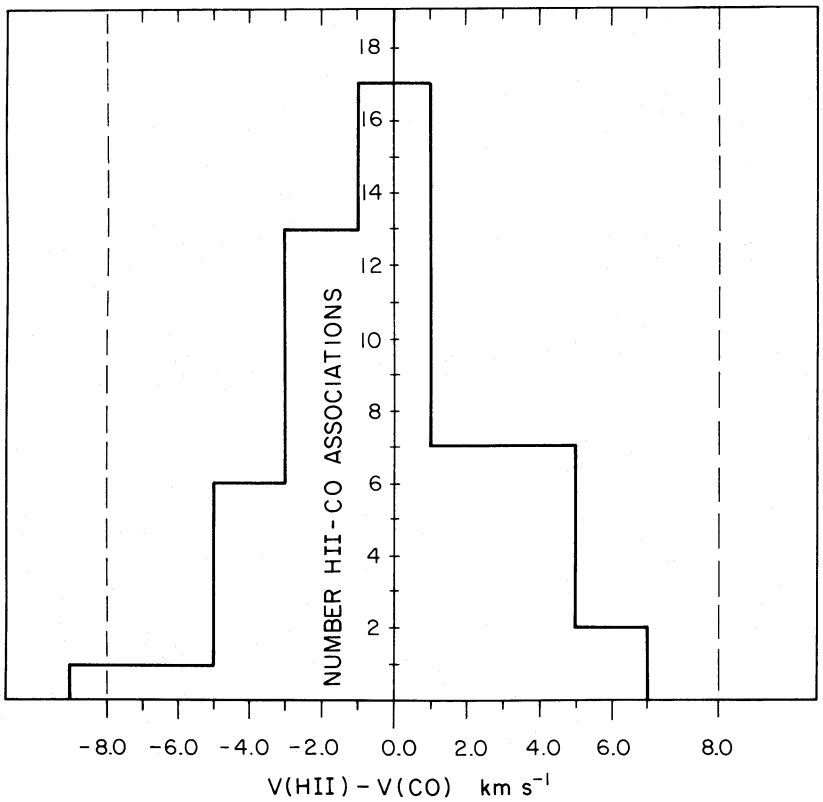

FIG. 5.—The distribution of velocity differences between each H II region and its associated CO cloud. Vertical dashed lines indicate the range in velocity difference which is permitted by the kinematic selection criterion for association (see § III). Since the distribution rapidly falls off within this selected range, the cloud sample is scarcely biased by the selection process.

stars; or if they are essential, their effects must be more often felt deep inside the clouds than at the cloud surfaces.

This study received support under NSF grant AST 82-12252 to the Five College Radio Astronomy Observatory, which is operated with permission of the Metropolitan District Commission, Commonwealth of Massachusetts. D. P. C. acknowledges the support received as a Bok fellow (1985–1986). D. B. S. was supported by NASA through the *IRAS* Extended Mission Program. We thank M. Brewer and M. Heyer for their helpful comments.

REFERENCES

Altenhoff, W. J., Downes, D., Pauls, T., and Schraml, J. 1978, *Astr. Ap. Suppl.*, **35**, 23.
Downes, D., Wilson, T. L., Bieging, J., and Wink, J. 1980, *Astr. Ap. Suppl.*, **40**, 379.
Fich, M., Treffers, R. R., and Blitz, L. 1982, in *Regions of Recent Star Formation*, ed. R. S. Roger and P. E. Dewdney (Dordrecht: Reidel), 201.
Habing, H. J., and Israel, F. P. 1979, *Ann. Rev. Astr. Ap.*, **17**, 345.
Herbst, W., and Assousa, G. E. 1977, *Ap. J.*, **217**, 473.
Israel, F. 1978, *Astr. Ap.*, **70**, 769.
Jones, B. F., and Herbig, G. H. 1979, *A.J.*, **84**, 1872.
Lockman, F. J. 1979, *Ap. J.*, **232**, 761.
Myers, P. C., Dame, T. M., Thaddeus, P., Cohen, R. S., Silverberg, R. F., Dwek, E., and Hauser, M. G. 1986, *Ap. J.*, **301**, 398.
Sanders, D. B., Clemens, D. P., Scoville, N. Z., and Solomon, P. M. 1986, *Ap. J. Suppl.*, **60**, 1.
Sanders, D. B., Scoville, N. Z., and Solomon, P. M. 1985, *Ap. J.*, **289**, 373.
Scoville, N. Z., and Solomon, P. M. 1973, *Ap. J.*, **180**, 131.
———. 1975, *Ap. J. (Letters)*, **199**, L105.
Scoville, N. Z., Yun, M. S., Clemens, D. P., Sanders, D. B., Solomon, P. M., and Waller, W. H. 1987, in press.

DAN P. CLEMENS: Steward Observatory, University of Arizona, Tucson, AZ 85721

DAVID B. SANDERS: Downs Laboratory, 320-47, California Institute of Technology, Pasadena, CA 91125

NICK Z. SCOVILLE: Department of Astronomy, 105-24, California Institute of Technology, Pasadena, CA 91125

WILLIAM H. WALLER: Five College Astronomy Department, University of Massachusetts, Amherst, MA 01003